Laser and Particle Beams (2001), *19*, 5–13. Printed in the USA.

Relativistic laser propagation through underdense and overdense plasmas

O. WILLI,[1] D.H. CAMPBELL,[1] A. SCHIAVI,[1] M. BORGHESI,[2] M. GALIMBERTI,[3] L.A. GIZZI,[3] W. NAZAROV,[4] A.J. MACKINNON,[5] A. PUKHOV,[6] AND J. MEYER-TER-VEHN[6]

[1]The Blackett Laboratory, Imperial College, SW7 2BZ, London, UK
[2]Department of Pure and Applied Physics, The Queen's University, Belfast, Northern Ireland
[3]IFAM-CNR, 56100 Pisa, Italy
[4]Chemistry Department, University of Dundee, UK
[5]Lawrence Livermore National Laboratory, Livermore, CA, USA
[6]Max-Planck-Institut fur Quantenoptik, Garching, Germany

(RECEIVED 24 January 2001; ACCEPTED 5 February 2001)

Abstract

Detailed investigations of the propagation of an ultraintense picosecond laser pulse through preformed plasmas have been carried out. An underdense plasma with peak density around $0.1n_c$ was generated by exploding a thin foil target with an intense nanosecond laser pulse. The formation of plasma channels with an ultraintense laser pulse due to ponderomotive expulsion of elections and the subsequent Coulomb explosion were investigated. The laser transmission through underdense plasmas was measured for a picosecond pulse at intensities above 10^{19} W/cm^2 with and without a plasma channel preformed with an ultraintense prepulse. The energy transmitted through the plasma increased from the few percent transmittance measured in absence of the preformed channel to almost 100% transmission with the channelling to main pulse delay at around 100 ps. The propagation of a relativistic laser pulse through overdense plasmas was also investigated. A well-characterized plasma with an electron density up to $8n_c$ was generated by soft X-ray irradiation of a low-density foam target. The propagation of the laser pulse was observed via X-ray imaging and monitoring the energy transmission through the plasma. Evidence of collimated laser transport was obtained.

1. INTRODUCTION

The fast ignitor (FI) approach (Tabak *et al.*, 1994) to inertial confinement fusion (ICF) motivates much of the present interest in ultraintense laser–plasma interaction studies. The scheme relies on the energy of an extremely intense laser pulse to start ignition in a compressed ICF capsule. It is necessary for this ignitor pulse to propagate through the coronal plasma, which ranges from underdense to 100 times critical over a scale of 100 μm. The scheme proposes the use of an ultraintense pulse prior to the ignition pulse to create a plasma channel extending into the overdense region, through which the ignition pulse can propagate. In order to study the feasibility of this, several issues have to be addressed, in particular, the formation of stable channels in underdense plasma and the propagation of ultraintense pulses in such channels. Also of importance is the propagation of the pulse into overdense plasma via induced transparency and hole-boring effects. The study of the propagation of ultraintense laser pulses through dense plasmas is therefore of great relevance to the success of the FI scheme. In addition, such studies are of great interest for fundamental physics issues in the relativistic regime.

Several experiments have studied propagation through underdense plasmas and channel formation in the relativistic regime (Young & Bolton, 1996; Borghesi *et al.*, 1997; Fuchs *et al.*, 1998*a*). Some experiments (Krushelnick *et al.*, 1997; MacKinnon *et al.*, 1998, 1999) have also demonstrated efficient guiding of intense pulses in a channel.

Investigation of propagation in overdense plasmas so far has been, for the most part, limited to computational modelling (Pukhov & Meyer-ter-Vehn, 1997) and interaction with thin foils or plasmas preformed at the surface of solids (Fuchs *et al.*, 1998*b*; Giulietti *et al.*, 1997; Zepf *et al.*, 1996; Kodama *et al.*, 1996).

This article reviews results obtained in an experimental campaign carried out over the past few years at the VULCAN laser facility, Rutherford Appleton Laboratory (UK). In the chirped pulse amplification (CPA) mode, the VULCAN laser is now capable of providing up to 75 J in 1-ps pulses at a wavelength of 1.054 μm. The propagation of relativistic

Address correspondence and reprint requests to: Oswald Willi, Imperial College of Science, Technology, and Medicine, SW7 2BZ, London, UK. E-mail: willi@ic.ac.uk

https://doi.org/10.1017/S0263034601191019 Published online by Cambridge University Press

intense pulses through preformed plasmas was investigated in the experiments. As the CPA energy output deliverable by the VULCAN laser has grown considerably in recent years, the first investigations performed by our group in this research area used 10–20 TW pulses, while measurements we have carried out more recently have employed pulses with power in excess of 50 TW. Using these pulses, propagation in two separate density regimes has been studied, with interaction of the laser with plasmas both underdense and several times critical. Overdense plasmas were preformed with a novel technique using soft X-ray preheating of low-density foam targets. Simulations indicate interaction with overdense regions 50–200 μm in length. The analysis and the interpretation of the data are currently in progress. In the following sections, the aims of the experiments, the techniques employed, and the main results obtained will be briefly described.

2. EXPERIMENTAL SETUP

The initial investigation of ultraintense propagation and channel formation in the underdense regime (Borghesi *et al.*, 1997, 1998) were performed with a 10-TW interaction pulse, and employed a single 400-ps pulse, frequency doubled to $\lambda = 0.527$ μm to preform underdense plasmas ahead of the interaction. This heating beam was focused onto target, in a spot between 200 and 300 μm in diameter, at an irradiance below 10^{13} W/cm^2. The interaction beam was focused in a 12–15 μm full width at half maximum (FWHM) focal spot. With an average interaction power of 10 TW, an incident irradiance between 5 and 9×10^{18} W/cm^2 was obtained. The delay between heating and interaction pulses was varied, allowing interaction with the plasma at different stages of its evolution. A fraction of the CPA pulse was frequency doubled and used as a transverse optical probe, performing Schlieren and interferometry.

The more recent investigations (Borghesi *et al.*, 2000; Campbell *et al.*, 2000) of laser propagation in the two density regimes employed a CPA pulse in excess of 50 TW, focused onto a target with an f/3.5 off-axis parabolic mirror. This produced a vacuum irradiance up to 5×10^{19} W/cm^2 (about 50 J on target, with up to 50% of the energy in a 10–15 μm focal spot). Two 1-ns laser pulses, frequency doubled to 0.527 μm, were used as heaters to preform the plasma, producing a total irradiance of about 5×10^{14} W/cm^2. A small fraction of the CPA pulse was frequency quadrupled and used as a transverse optical probe with a temporal resolution of 1–3 ps. The probe delay relative to the main pulse was controlled to within a few picoseconds. An f/4 UV objective was used to image the target on photographic film.

2.1. Channelling in underdense plasma

Underdense plasmas in the experiments were produced by exploding thin plastic foils 0.1 μm to 0.5 μm thick, with one or two 0.527-μm heating beams. After a suitable delay (typically of the order of 1 ns), the CPA pulse was focused into the plasma. At this time, the peak density of the plasma was below $n_c/10$ and its longitudinal extension was of the order of a millimeter. In the later experiments, a fraction of the energy of the main CPA pulse was used to provide a prepulse, collinear with the main pulse. The prepulse could be focused into the plasma ahead of the main pulse and used to open a density channel.

Interferometry was performed along the transverse optical probe line using a modified Nomarsky interferometer (Benattar *et al.*, 1979). Other diagnostics included imaging of the transmitted laser spot, forward and back-scatter spectroscopy and γ-ray measurements. The transmitted laser light was split with an uncoated glass window and a fraction collected with an f/2.5 lens, which imaged the focal plane of the parabola onto an optical CCD camera in order to image the transmitted portion of the main laser pulse. A calorimeter placed behind the window measured the laser energy transmitted through the plasma (Fig. 1b).

2.2. Overdense plasma interaction

Overdense plasmas were produced by soft X-ray ionization of foam targets. Triacrylate and CH foams of different densities and lengths were used. The triacrylate foams were 50 μm thick with density 10 or 20 mg/cc and were mounted in washers with a parylene backing. The CH foams were free-standing and had densities of 30 or 50 mg/cc and lengths from 100 to 250 μm. Two gold burn-through foils (700 Å of gold on 1 μm formvar) were positioned 50 μm in front of the foam, 200 μm apart. The two heating beams were focused onto the gold foils. The soft X-ray emission from the foils (Kania *et al.*, 1992) was used to heat and ionize the foam target (Afshar-rad *et al.*, 1994) to produce the required plasma conditions. Interaction with such plasmas can be reliably simulated with PIC codes. The CPA pulse was focused onto the preheated foam after a delay in the range of 800 to 1500 ps, which allowed adequate ionization and expansion of the foam.

Several additional diagnostics were run during each shot to provide information on the plasma formation and laser interaction. X-ray pinhole cameras with 25-μm pinholes were placed in front of and behind the target (Fig. 2). The cameras were loaded with Kodak Industrex X-ray film. A 7.5-μm Be foil was used as a filter, blocking radiation below 500 eV. The transverse optical probe was used in a shadowgraphy arrangement to observe the evolution of the rear of the foam target.

3. EXPERIMENTAL RESULTS

3.1. Channelling in underdense plasmas

Self-channelling of the 10-TW CPA pulse appeared to be a typical feature of the interaction in the investigated experimental conditions and was detected via optical probe

https://doi.org/10.1017/S0263034601191019 Published online by Cambridge University Press

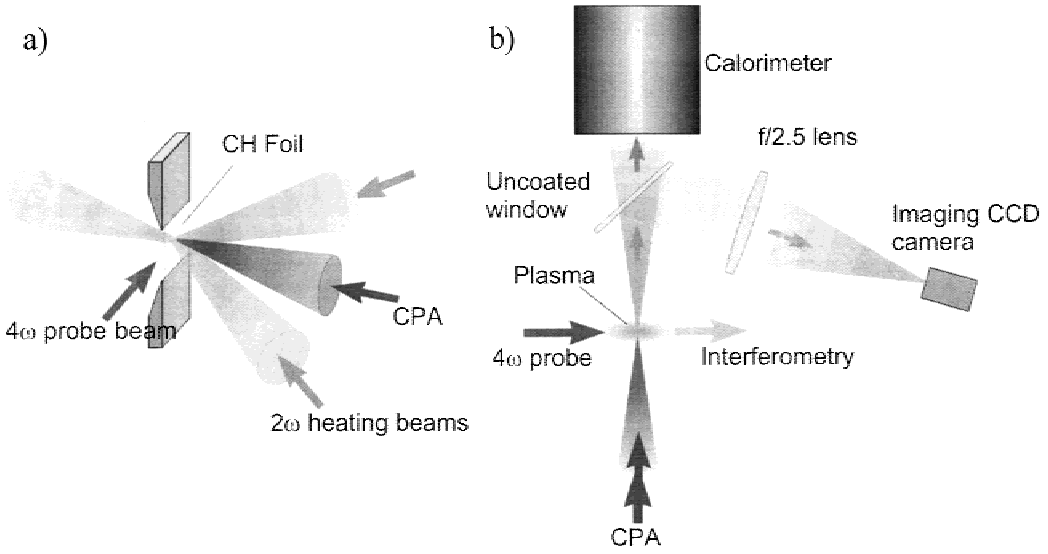

Fig. 1. (a) Target and laser arrangement for underdense interaction studies. (b) A schematic of the diagnostic setup.

measurements. In Figure 3, the spatially resolved second harmonic radiation emitted during the interaction of a 10-TW pulse with the preformed plasma is shown. The measured density profile is also presented (1-D simulations predict that the plasma is fully ionized, with a peak density of about $5\times10^{20}/\mathrm{cm}^3$). The channel-like emission is time-integrated and is due to second harmonic (2ω) light emitted during the interaction, produced via nonlinear processes in correspondence with the large density and intensity gradients present inside the channel. It can therefore be interpreted as a signature of the spatial extent of the interaction beam in the plasma. The average diameter of the channel is about 5 μm and its length about 130 μm. The channel changes in size periodically over distances of 15–20 μm with the transverse dimension varying within a few microns. From comparison with the preformed plasma profile, it can be seen that the laser pulse focuses down to 5 μm in size at a density of around 0.05 times the critical density n_c ($n_c\sim1\times10^{21}$ cm^{-3} for $\lambda=1$ μm). It should also be noted that the laser power was about 25 times the threshold power for relativistic self-focusing, $P_{th}=17\omega^2/\omega_p^2\cong0.4$ TW at this density.

Evidence of channelling was also obtained from interferometric measurements. The interferogram of Figure 4 was taken at about 5 ps after the interaction (the preformed plasma density profile is also shown). A front (due to the shock wave expanding in the preformed plasma) produced by the short pulse while focusing down into the channel is clearly visible. The laser pulse appears to be focused with an f/4.5

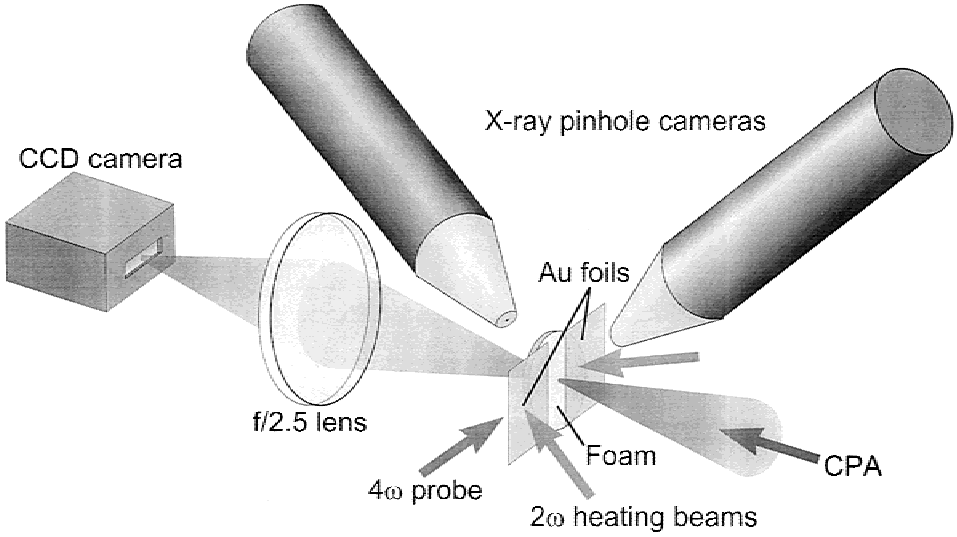

Fig. 2. Beam and diagnostic arrangement for overdense interaction studies.

https://doi.org/10.1017/S0263034601191019 Published online by Cambridge University Press

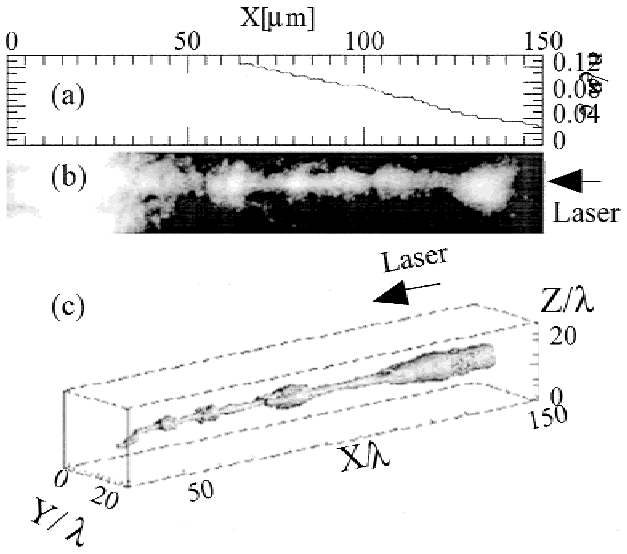

Fig. 3. (a) Density profile of plasma. (b) 2ω self-emission image of channel. (c) 3-D PIC simulation results.

cone up to a background density of approximately $0.07 n_c$ at a distance of about 200 μm from the original target position. Beyond that density, it self-focuses into the channel. At the time the interferogram was taken, the density channel formed by the short pulse had already expanded to a size of about 25 μm in diameter.

The experiment has been simulated with the 3-D PIC code VLPL (Virtual Laser Plasma Laboratory) developed at the Max Planck Institute (Garching) for massive parallel processing (MPP). The density profile and beam parameters of the experimental case of Figure 3 were used. The simulation box is shown in Figure 3c. The laser pulse (λ = 1.054 μm), polarized in the Z direction, is incident from the right with an incident irradiance of $I_0 = 8 \times 10^{18}$ W/cm^2 and

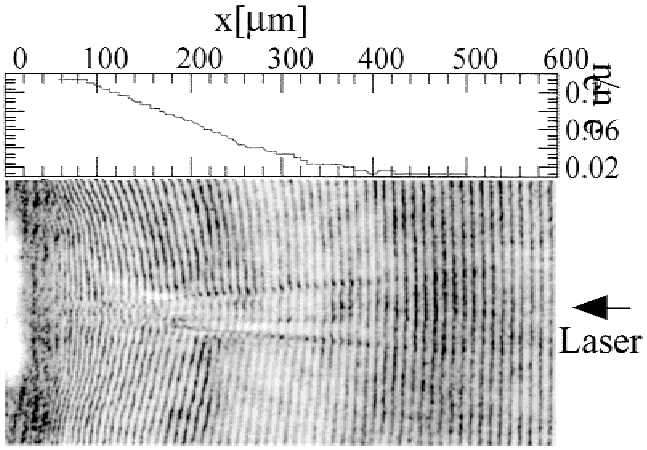

Fig. 4. Interferogram 5 ps after CPA interaction under conditions similar to Figure 3.

a 12λ (FWHM) transverse Gaussian profile, giving a power of 10 TW. The intensity distribution $\langle I \rangle$ is shown for a time close to the peak of the pulse. After an initial unstable phase, the incident beam self-focuses into a narrow single channel at a density of about $0.07 n_c$, according to the process described by Pukhov and Meyer-ter-Vehn (1996). The channel width pulsates as the pulse defocuses and refocuses with a characteristic period of 15–30 λ. These results closely reproduce the experimental observations.

The channel of Figure 3(c) is further analyzed in Figure 5 by plotting the electron density for a Y, Z cross section at $X = 80\ \lambda$ and also as a line profile, normalized to the critical density n_c. One observes that electrons are expelled from the channel region and form a radially outgoing shock. After the pulse has traversed the plasma, a collisionless shock forms due to the ponderomotive expulsion of electrons and (consequently) of ions, and the channel quickly expands. The channel expansion has been studied using time-resolved interferometry. The plasma density at the center of the channel is a fraction (variable between 0.1 and 0.4) of the background density. The channel edges move out with an initial speed of about 5×10^8 cm/s, and expands with time following a $t^{1/2}$ dependence, as predicted from shock waves theory (Zel'dovich and Raizer, 1966).

3.2. Guiding through preformed plasma channels

The propagation of the main CPA pulse through underdense plasma at a 50-TW level was first studied without a preformed plasma channel. The energy transmission through

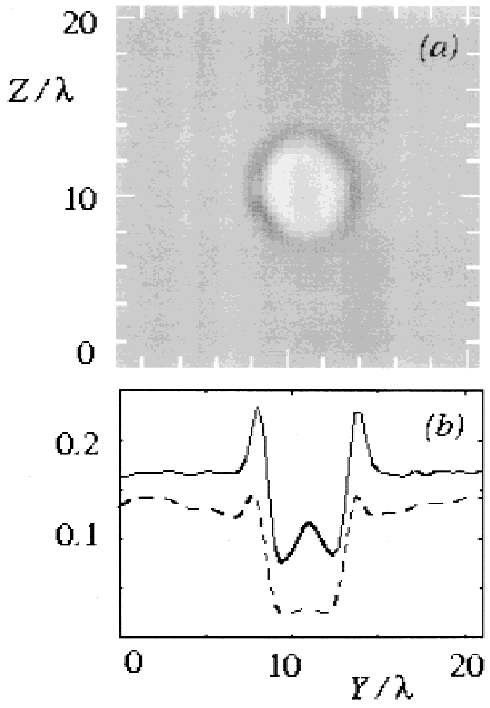

Fig. 5. Electron density in units of n_c for Y–Z plane at $X = 80\lambda$.

https://doi.org/10.1017/S0263034601191019 Published online by Cambridge University Press

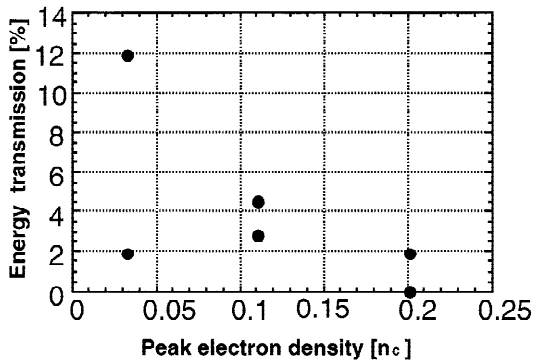

Fig. 6. Transmission of CPA pulse energy versus peak density in long-scale underdense plasmas.

the plasma in this case was very low, as seen in Figure 6. The peak densities were estimated using the model of London and Rosen (1986). Even when using the 0.1-μm target, which gave a plasma with peak density of a few times $n_c/100$, the energy transmitted was limited to a few percent of the laser energy incident on target. This is consistent with numerical simulations (Chessa *et al.*, 1998) and previous experiments (Cobble *et al.*, 1997), which have reported anomalously high laser absorption even in very underdense plasmas for relativistically intense laser pulses.

Reduction in energy transmission may also be related to the onset of relativistic filamentation rather than whole-beam self-focusing (Young *et al.*, 1995. Wang *et al.*, 2000). Relativistic filamentation can cause spreading of the beam energy at angles much larger than the focusing angle. Filamentation and beam spreading were indeed observed in the experiment, as seen, for example, in Figure 7, showing an interferogram taken 5 ps after the interaction of a 50-TW pulse with the plasma. The dashed white line indicates the angle of the cone defined by the focusing optics (f/3.5). Some of the filaments appear to diverge at angles larger than the collection angle (about f/3.5) of the calorimeter. Filamentation is even more evident in Figure 7b, showing the second image of the interaction region of the same interferogram of Figure 7a. As the fringes on this second image were coarser, the image can be interpreted as a shadowgram of the interaction region. Filaments breaking into other filaments can be seen. This behavior was not observed for the previous experiment for 10–20 TW in which a single self-focused filament was observed (Borghesi *et al.*, 1997, 1998). This, together with observations at varying intensities carried out in the present experiment, suggests a transition between two different regimes of interaction (whole beam self-channelling to relativistic filamentation) taking place in the 20–50 TW intensity range.

The effect of the presence of a preformed channel on the propagation of the main pulse was investigated. The channel was formed by focusing into the plasma the prepulse, with a prepulse-to-main ratio of 1:2. The intensity of the prepulse was also above 10^{19} W/cm^2, and a rapidly expanding channel was formed, as observed in the previous experiments (Borghesi *et al.*, 1997, 1998). The interaction of the 25-TW pulse with the plasma appeared to be less affected by filamentation than for the 50-TW pulse case. An interferogram showing the channel 45 ps after its formation can be seen in Figure 8.

The main CPA pulse was focused into the channel at various stages of the channel expansion, and the CPA main pulse transmittance was measured, for various plasma conditions, as a function of the delay between the main and the channelling pulse. A clear increase in energy transmission was observed, as visible for example in the graph shown in Figure 9, where the energy transmission is plotted with channel radius. The energy transmitted through the plasma grows from the few percent transmittance measured in the absence of a preformed channel (corresponding to zero delay) to

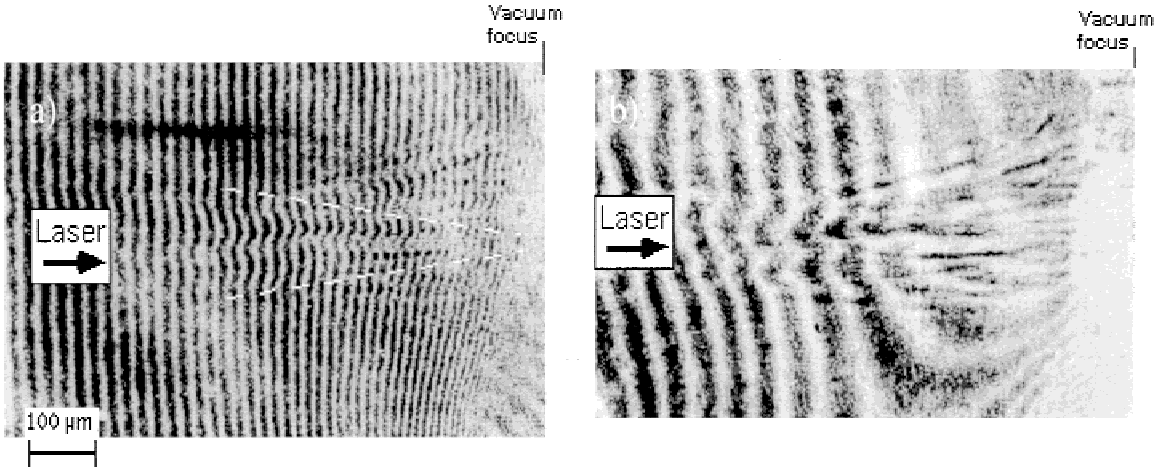

Fig. 7. Details of an interferogram taken 5 ps after the propagation of a 50-TW pulse through a laser beam. The two images (from the same interferogram) both show the interaction region. Laser breakup and formation of filaments are clearly visible.

https://doi.org/10.1017/S0263034601191019 Published online by Cambridge University Press

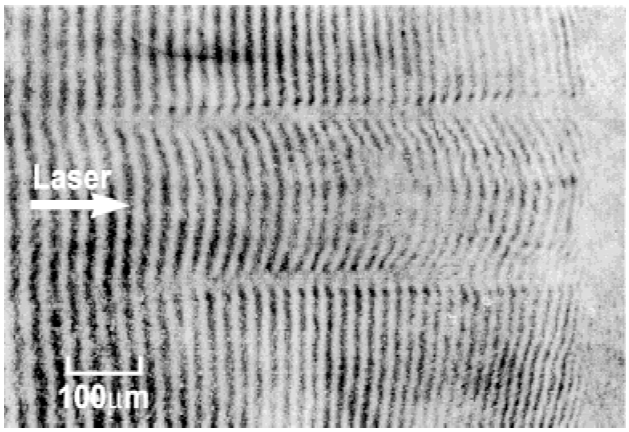

Fig. 8. Interferogram of the channel taken 45 ps after its formation.

about 90% transmission when the channelling-to-main delay is of the order of 100 ps.

Although a detailed analysis of the data has still to be done, a number of preliminary considerations can be made. First, one has to take into account the energy distribution in the focal plane of the laser. Typically, only 50% of the energy is contained in the small size central spot (10–20 μm diameter), and this determines an intensity exceeding 10^{19} W/cm^2 in this spot. The rest of the energy is distributed throughout lower intensity wings extending around the central spot (a systematic characterization of the focal spot may be required, as was done a few years ago (Danson *et al.*, 1998). Therefore, efficient propagation of the energy contained in the high intensity spot is achieved even after 30 ps, with more than half of the energy transmitted through the plasma. The factors leading to increased transmission are substantially two: (1) the fact that the density profile across the channel acts as a positive lens on the main pulse propagating through it, limiting the diffraction of the beam; (2) the fact that the density inside the channel is significantly lower than the background plasma. This leads to decreased absorption and also reduces the effect of relativistic filamentation (as the threshold for relativistic self-focusing $P \propto n_c/n_e$ is increased).

The transmitted energy increase when the channelling-to-main delay is increased may be explained by the fact that, as the channel expands, the low intensity, larger diameter wings of the focal spot are encompassed by the channel walls. The internal dynamics of the channel (e.g., the temporal evolution of the density inside the channel) will also play a role. Detailed modeling and data analysis are required to determine the relative importance of the different factors.

3.3. Interaction with overdense plasma

Typical results of the overdense interaction investigations are shown in the following. The imaging of the rear of the target onto a CCD shows an emission of radiation from the rear for several of the lower density foams (Fig. 10). A compact spot is seen corresponding to the position of the laser focal spot. This is observed only through foams 50 μm thick with density of 20 or 10 mg/cc. As the unheated foams are optically transparent and the CCD image was time-integrated, there was some doubt that the transmitted light could come from the low intensity pedestal (ASE) preceding the main pulse. However, when only the ASE of the main pulse was fired with the same heating conditions, no compact, bright spot was observed. The optical CCD was calibrated with a low energy shot (0.1 J). From this it is estimated that this radiation accounts for less than 10^{-5} of the energy of a full power shot of ~20 J. Figure 10b shows a CCD image from a shot on

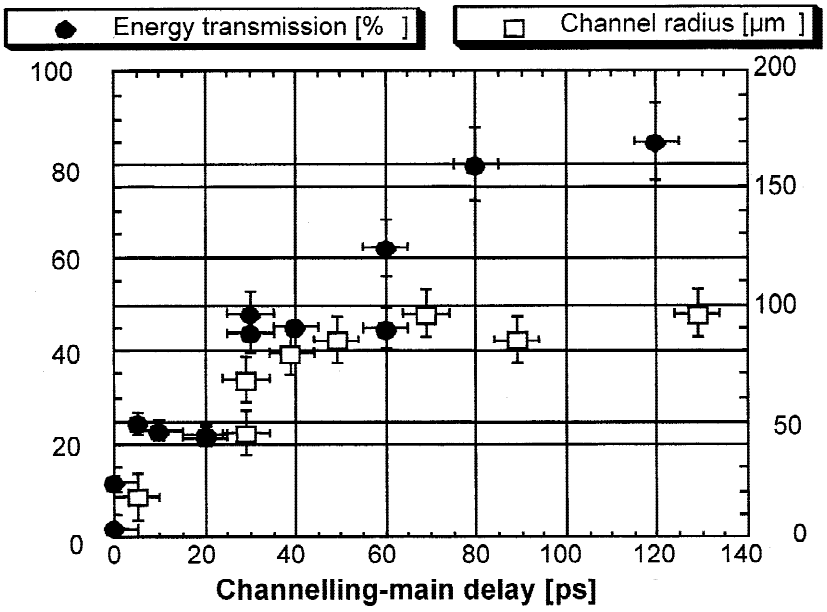

Fig. 9. Energy transmission through an underdense plasma (peak density $\approx 0.03n_c$, length $\approx$ 1–2 mm, obtained for 0.1 μm) in the presence of a preformed channel. The transmission is plotted versus the delay between the channel formation and the propagation of the main pulse. The temporal evolution of the channel radius is also plotted.

https://doi.org/10.1017/S0263034601191019 Published online by Cambridge University Press

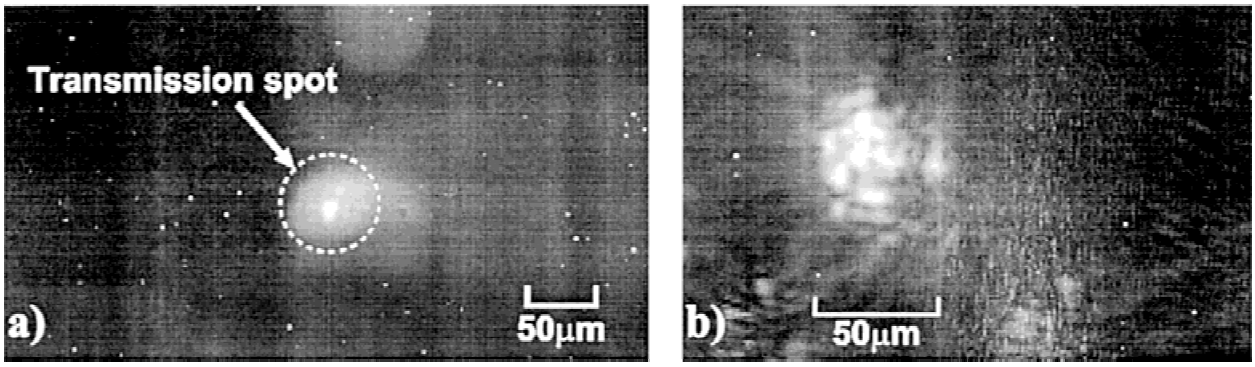

Fig. 10. CCD images of target rear, transmission observed through a 50-μm-long, 20-mg/cc foam (a) and a 200-μm-long, 30-mg/cc foam (b).

a 30 mg/cc foam 200 μm in length. A breakup of the spot can be seen, over an area 50 μm in diameter.

X-ray images from the rear and front pinhole cameras (Figure 11) show bright filaments extending through the foam and some distance beyond. The film shows the bright spots of the heating beams on the foils with a vertical filament in the center. Such filaments are observed on several shots for different foam densities and lengths. In rare cases, breaking up of the filaments at the rear of the foam was observed. Transverse optical probing reveals a localized region of expanding plasma at the rear of the foam, which lines up with the self-emission from the CPA interaction at the front. This localized expansion implies a collimated transport of energy through the foam.

4. MODELING AND DISCUSSION

Plasma simulations have been run using the 1-D Lagrangian hydrocode MEDUSA to determine the electron density of the plasma at the time of laser interaction. Results (Fig. 12) show a uniform ionization with an electron density profile peaking for all target types at around $8n_c$. The electron density remains above critical density for a length similar to the unexploded foam length.

The X-ray filaments within the plasma could be produced by heating of the plasma from the laser as it propagates through the overdense plasma. This is possible in the high intensity regime due to induced transparency (Kaw & Dawson, 1970), relativistic modification of critical density, or

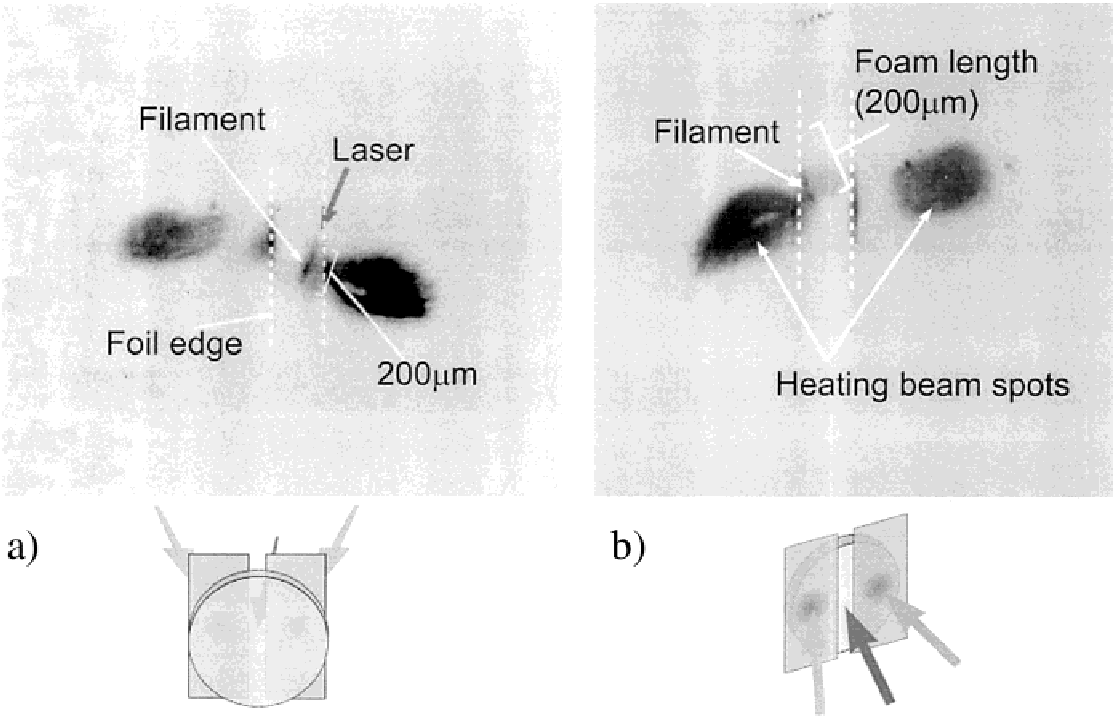

Fig. 11. Soft X-ray image from a rear pinhole camera (a) and a front camera (b) with overlay showing the position of the surfaces of the foam and the gold foils.

https://doi.org/10.1017/S0263034601191019 Published online by Cambridge University Press

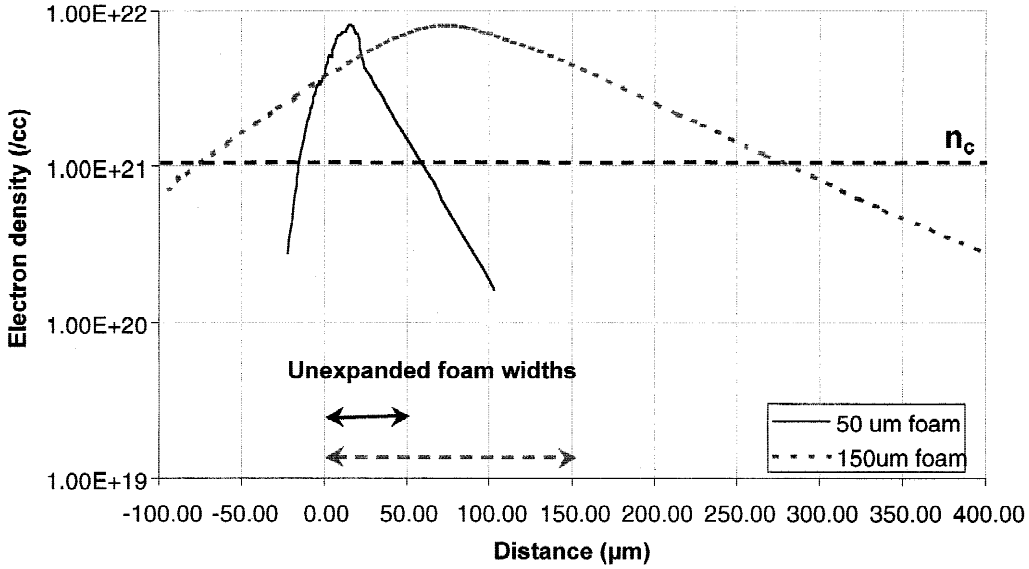

Fig. 12. Simulated electron density profiles for 50-μm (solid line) and 150-μm (dashed line) foams at the time of CPA interaction.

hole boring (Wilks *et al.*, 1992) due to ponderomotive pressure. As the electron density was $8n_c$, induced transparency could only take place if self-focusing of the CPA pulse increased the laser intensity. Alternatively, the filaments could be produced by a stream of fast electrons, accelerated by the laser. In fact, localized expansion at the rear of the target has been attributed, in the past (Tatarakis *et al.*, 1998), to fast electrons emerging from the target. PIC simulations are planned to discriminate between the various mechanisms that could be responsible for the observed results.

5. CONCLUSIONS

The propagation and transmission of relativistically intense picosecond pulses through underdense plasmas has been studied for different plasma conditions. The results of a series of experiment performed using the CPA VULCAN pulses indicated that the propagation of 10–20-TW pulses at relativistic intensity through preionized plasmas is characterized by relativistic self-channelling. This phenomenon was detected using optical probing diagnostics, and modeled using 3-D PIC simulations that closely reproduced the experimental results. Filamentation and laser breakup were observed when the laser power was raised at a 50-TW level.

The energy transmission measured was low even through very underdense plasmas. However, the transmission was greatly improved when a channel was preformed ahead of the main laser pulse, using a fraction of the energy of the pulse itself. Under the right conditions, up to 85–90% of the laser energy on target could be propagated through the plasma. These measurements have obvious relevance to fast ignition. In particular, the measurements stress the importance of the presence of a preformed density channel in order to achieve efficient energy propagation through the plasma at ultrahigh intensity. In fact, in the absence of a preformed channel the millimeter-sized coronal plasma surrounding the compressed core of the imploded capsule would be able to absorb most of the energy transported by the pulse.

In the overdense regime, X-ray emission from the plasma suggests collimated transport of energy. This is supported by localized expansion of the rear and optical images of the emission from the target. This energy transport is possibly due to relativistic electrons; however further study is necessary to clarify the mechanisms at work in this regime.

ACKNOWLEDGMENTS

Our thanks go to the staff of the Central Laser Facility for their assistance and support throughout the experiment. The experiments were funded by an EPSRC grant.

REFERENCES

Afshar-rad, T., Desselberger, M., Dunne, M., Edwards, J., Foster, J.M., Hoarty, D., Jones, M.W., Rose, S.J., Rosen, P.A., Taylor, R. & Willi, O. (1994). *Phys. Rev. Lett.* **73**, 74.

Benattar, R., Popovics, C. & Siegel, R. (1979). *Rev. Sci. Instrum.* **50**, 1583.

Borghesi, M., MacKinnon, A.J., Barringer, L., Gaillard, R., Gizzi, L.A., Meyer, C., Willi, O., Pukhov, A. & Meyer-ter-Vehn, J. (1997). *Phys. Rev. Lett.* **78**, 879.

Borghesi, M., MacKinnon, A.J., Gaillard, R., Willi, O., Pukhov, A. & Meyer-ter-Vehn, J. (1998). *Phys. Rev. Lett.* **80**, 5137.

Borghesi, M., Schiavi, A., Campbell, D.H., Willi, O., Galim-

https://doi.org/10.1017/S0263034601191019 Published online by Cambridge University Press

berti, M. & Gizzi, L.A. (2000). *CLF ANNUAL Report*, **RAL-TR-2000-034** Rutherford Appleton Laboratory.

Campbell, D.H., Schiavi, A., Willi, O., Borghesi, M., Mackinnon, A.J., Galimberti, M., Gizzi, L.A. & Nazarov, W. (2000). *CLF ANNUAL Report*, **RAL-TR-2000-034** Rutherford Appleton Laboratory.

Chessa, P., Mora, O. & Antonsen Jr, T.M. (1998). *Phys. Plasmas* **5**, 3451.

Cobble, J.A., Johnson, R.P. & Mason, R.J. (1997). *Phys. Plasmas* **4**, 3006.

Danson, C.N., Collier, J., Neely, D., Barzanti, L.J., Damerell, A., Edwards, C.B., Hutchinson, M.H.R., Key, M.H., Norreys, P.A., Pepler, D.A., Ross, I.N., Taday, P.F., Toner, W.T., Trentelman, M., Walsh, F.N., Winstone, T.B. & Wyatt, R.W.W. (1998). *J. Mod. Opt.* **45**, 1653.

Fuchs, J., Adam, J.C., Amiranoff, F., Baton, S.D., Gallant, P., Gremillet, L., Héron, A., Kieffer, J.C., Laval, G., Malka, G., Miquel, J.L., Mora, P., Pépin, H. & Rousseaux, C. (1998*b*). *Phys. Rev. Lett.* **80**, 2326.

Fuchs, J., Malka, G., Adam, J.C., Amiranoff, F., Baton, S.D., Blanchot, N., Heron, A., Laval, G., Miquel, J.L., Mora, P., Pepin, H. & Rousseaux, C. (1998*a*). *Phys. Rev. Lett.* **80**, 1658.

Giulietti, D., Gizzi, L.A., Giulietti, A., Macchi, A., Teychenné, D., Chessa, P., Rousse, A., Gheriaux, G., Chambaret, J.P. & Darpentigny, G. (1997). *Phys. Rev. Lett.* **79**, 3194.

Kania, D.R., Kornblum, H., Hammel, B.A., Seely, J., Brown, C., Feldman, U., Glendinning, G., Young, P., Hsieh, E., Hennesian, M., Dasilva, L., Macgowan, B.J., Montgomery, D.S., Back, C.A., Doyas, R., Edwards, J. & Lee, R.W. (1992). *Phys. Rev. A* **46**, 7853.

Kaw, P. & Dawson, J. (1970). *Phys. Fluids* **13**, 472.

Kodama, R., Takahashi, K., Tanaka, K.A., Tsukamoto, M., Hashimoto, H., Kato, Y. & Mima, K. (1996). *Phys. Rev. Lett.* **77**(24), 4906.

Krushelnick, K., Ting, A., Moore, C.I., Burris, H.R., Esarey, E., Sprangle, P. & Baine, M. (1997). *Phys. Rev. Lett.* **78**, 4047.

London, R.A. & Rosen, M.D. (1986). *Phys. Fluids* **29**, 3813.

Mackinnon, A.J., Borghesi, M., Gaillard, R., Malka, G., Willi, O., Offenberger, A.A., Pukhov, A., Meyer-ter-Vehn, J., Canaud, B., Miquel, J.L. & Blanchot, N. (1999). *Phys. Plasmas* **6**, 2185.

Mackinnon, A.J., Borghesi, M., Iwase, A. & Willi, O. (1998). *Phys. Rev. Lett.* **80**, 5349.

Miquel, L. & Blanchot, N. (1999). *Phys. Plasmas* **6**, 2185.

Pukhov, A. & Meyer-ter-Vehn, J. (1996). *Phys. Rev. Lett.* **76**, 3975.

Pukhov, A. & Meyer-ter-Vehn, J. (1997). *Phys. Rev. Lett.* **79**, 2686.

Tabak, M., Hammer, J., Glinsky, M.E., Kruer, W.L., Wilks, S.C., Woodworth, J., Campbell, E.M., Perry, M.D. & Mason, R.J. (1994). *Phys. Plasmas* **1**, 1626.

Tatarakis, M., Davies, J.R., Lee, P., Norreys, P.A., Kassapakis, N.G., Beg, F.N., Bell, A.R., Haines, M.G. & Dangor, A.E. (1998). *Phys. Rev. Lett.* **81**, 999.

Wang, X., Krishnan, M., Saleh, N., Wang, H. & Umstadter, D. (2000). *Phys. Rev. Lett.* **84**, 5324.

Wilks, S.C., Kruer, W.L., Tabak, M. & Langdon, A.B. (1992). *Phys. Rev. Lett.* **69**, 1383.

Young, P.E. & Bolton, P.R. (1996). *Phys. Rev. Lett.* **77**, 4556.

Young, P.E., Foord, M.E., Hammer, J.H., Kruer, W.L., Tabak, M. & Wilks, S.C. (1995). *Phys. Rev. Lett.* **75**, 1082.

Zel'dovich, Ya.B. & Raizer, Yu.P. (1966). *Physics of shock waves and high temperature hydrodynamic phenomena* Vol. 1, p. 97. New York: Academic Press.

Zepf, M., Castro-Colin, M., Chambers, D., Preston, S.G., Wark, J.S., Zhang, J., Danson, C.N., Neely, D., Norreys, P.A., Dangor, A.E., Dyson, A., Lee, P., Fews, A.P., Gibbon, P., Moustaizis S. & Key, M.H. (1996). *Phys. Plasmas* **3**, 3242.

https://doi.org/10.1017/S0263034601191019 Published online by Cambridge University Press